Asymptotic analysis of boundary-effect on strength of concrete

Kai Duan and Xiaozhi Hu*

School of Mechanical Engineering, University of Western Australia, 35 Stirling Highway, Crawley, WA 6009, Australia.

xhu@mech.uwa.edu.au, Fax: 61-8-9380-1024

ABSTRACT: A new size effect model is presented, which deals with the specimen boundary influence on the strength of concrete measured from the maximum load tests. The new boundary effect model shows that the size independent tensile strength and fracture toughness (and then the specific fracture energy) of concrete-like quasi-brittle composites can be conveniently determined from the simple maximum load tests. The common size effect observed using geometrically similar specimens is only a special case of the specimen boundary effect on fracture properties of concrete. The difference and similarity between the current boundary effect model and the common size effect models are discussed and illustrated with concrete results measured from four different sets of geometrically similar specimens. It is shown that the asymptotic analysis of the large plate with a small edge crack, for which the front specimen boundary rather than the specimen size needs to be considered, provides the solution to all the quasi-brittle fracture transition curves, or the size effect.

Keywords: boundary effect, size effect, strength, fracture toughness, fracture process zone, fracture energy

1 INTRODUCTION

The size effect on the strength and specific fracture energy of concrete remains one of the prime research subjects of fracture mechanics of concrete because of its fundamental significance and practicality. Geometrically similar specimens have commonly been used because under such a condition the size variation becomes the sole parameter and the size effect can thus be clearly defined. The size effect on the specific fracture energy G_f of concrete is dealt with specifically in a separate contribution to the conference (Duan et al, 2004). Therefore, the main focus of the present paper is on the nominal tensile strength of concrete and the associated size effect.

A recent research program at the University of Western Australia (Duan & Hu 2002, Hu 2002) has adopted a different approach to the size effect problem. By considering the influence of specimen boundary, rather than the size, on the strength behavior of concrete, a new boundary effect model is developed (Duan & Hu 2002, 2003a,b,c, Hu 2002).

The objective of this paper is to provide further theoretical verification to the boundary effect model, and to show that the size-independent tensile strength and fracture toughness and fracture energy of concrete can be determined using the size dependent quasi-brittle fracture results measured from the simple maximum load tests.

2 BOUNDARY EFFECT MODEL

2.1 *Two nominal strengths: σ_N and σ_n*

Two different nominal strengths can be defined, as shown in Figure 1, by the single-edge-notched-tension (SENT) and three-point-bend (3-p-b) specimens. The difference is that σ_N ignores the presence of the crack, and σ_n takes the presence of the crack into account although the stress concentration at the crack-tip is not considered. Let $\alpha = a/W$, it can be determined from Figure 1:

$$\sigma_N = \mathrm{A}(\alpha)\cdot\sigma_n = \begin{cases} \dfrac{(1-\alpha)^2}{1+2\alpha}\cdot\sigma_n & \text{SENT} \quad \text{(a)} \\ (1-\alpha)^2\cdot\sigma_n & \text{3-p-b} \quad \text{(b)} \end{cases} \tag{1}$$

$\mathrm{A}(\alpha)$ can be worked out for any specimen geometry although only the solutions for SENT and 3-p-b

specimens illustrated in Figure 1 are provided in Equation 1.

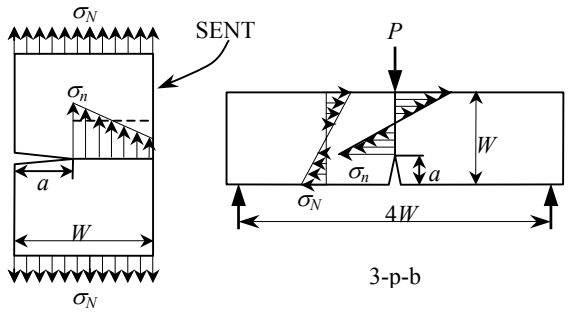

Figure 1. Two nominal strengths: σ_N does not consider the presence of the crack, and σ_n considers the presence of the crack. σ_n is used in the present boundary effect model.

For a large plate with the condition that $\alpha \approx 0$, $\sigma_N = \sigma_n$. σ_N is commonly used in the stress intensity factor formulae and the size effect models (Bažant 1984, Karihaloo et al 2003, Carpinteri 1994). σ_n is more useful for small specimen size W and for large α-ratio ($\rightarrow 1$) because it is related to the tensile strength f_t.

Different to the aforementioned size effect models using σ_N, the present boundary effect model uses σ_n.

2.2 *Boundary effect solution of large plate*

For simplicity, the SENT geometry illustrated in Figure 1 is considered. The large plate condition means that $\alpha \rightarrow 0$ and $\sigma_N = \sigma_n$. The quasi-brittle fracture transition has been determined previously for this special situation (Hu 1998, 2002, Hu & Wittmann 2000).

$$\sigma_n = \sigma_N = \frac{f_t}{\sqrt{1 + a/a_\infty^*}} \qquad (2)$$

$$a_\infty^* = \frac{1}{\pi \cdot Y^2} \cdot \left(\frac{K_{IC}}{f_t}\right)^2 = 0.25 \cdot \left(\frac{K_{IC}}{f_t}\right)^2$$

in which f_t is the tensile strength, K_{IC} is the fracture toughness, and the geometry factor $Y = 1.12$ for the large plate condition. The reference crack a^*_∞ defined in Equation 2 is obviously a material constant. The quasi-brittle fracture given by Equation 2 is illustrated in Figure 2 together with the two asymptotic limits: the tensile strength f_t and the fracture toughness K_{IC} criterion for the linear elastic fracture mechanics (LEFM) situation. These two asymptotic limits are given by Equation 2 for $a/a^*_\infty << 1$ and $a/a^*_\infty >> 1$, respectively.

Since the size of the large plate does not need to be considered because $\alpha \rightarrow 0$, the quasi-brittle fracture transition specified by Equation 2 and illustrated in Figure 2 is due purely to the influence of the specimen front face. The fracture process zone (FPZ) size (proportional to a^*_∞) and its distance to the specimen front face (given by the crack length a) determine the quasi-brittle fracture transition.

Interestingly, although Equation 2 models the boundary effect rather than the size effect, it will be proven in this paper that the size effect behaviors of finite-sized SENT specimens and specimens of other geometry and loading conditions are actually defined by the asymptotic boundary effect solution of the large plate.

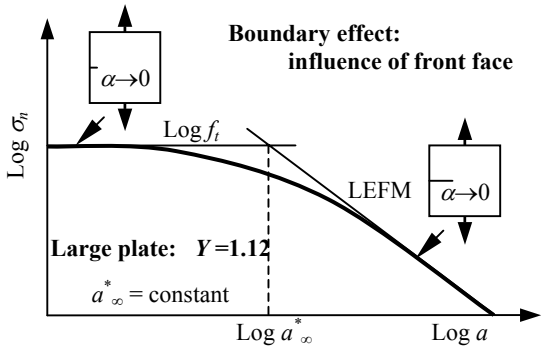

Figure 2. Asymptotic boundary effect curve for a large plate with a small edge crack. The specimen front face, rather than the specimen size, needs to be considered.

2.3 *Equivalent crack a_e of small specimen*

Section 2.2 shows that because of the specimen boundary influence, the fracture toughness K_{IC} criterion may not be applicable even if the specimen size is huge. The same boundary effect exists in small specimens, only more complicated, because similar to the front face the specimen back face can also influence the quasi-brittle fracture transition.

Let us consider a specimen where K_{IC} applies only at its center (e.g. $\alpha \approx 0.5$). Following LEFM,

$$K_{IC} = \sigma_N \cdot Y(\alpha) \cdot \sqrt{\pi a} \qquad (3)$$

Note that the nominal strength σ_N is used in Equation 3. From Equations 1 and 3, the nominal strength σ_n can be solved, i.e.

$$\sigma_n = \frac{K_{IC}}{\mathrm{A}(\alpha)\cdot Y(\alpha)\cdot\sqrt{\pi a}} = \frac{f_t}{\sqrt{\dfrac{\left(\dfrac{\mathrm{A}(\alpha)\cdot Y(\alpha)}{1.12}\right)^2\cdot a}{\dfrac{1}{1.12^2\pi}\cdot\left(\dfrac{K_{IC}}{f_t}\right)^2}}} = \frac{f_t}{\sqrt{\dfrac{\mathrm{B}(\alpha)\cdot a}{a^*_\infty}}} = \frac{f_t}{\sqrt{a_e/a^*_\infty}} \tag{4}$$

in which the equivalent crack a_e and B(α) are given by:

$$a_e = \mathrm{B}(\alpha)\cdot a$$
$$\mathrm{B}(\alpha) = \left(\frac{\mathrm{A}(\alpha)\cdot Y(\alpha)}{1.12}\right)^2 \tag{5}$$

In comparison with Equations 2 and 4 for $a/a^*_\infty >> 1$ and $a_e/a^*_\infty >> 1$, it is obtained (Duan & Hu 2003 a,b,c) that:

$$\sigma_n = \frac{f_t}{\sqrt{1 + a_e/a^*_\infty}} \tag{6}$$

If a specimen satisfies the large plate condition that $\alpha \to 0$, the equivalent crack a_e is the same as the real crack length a. As a result, Equation 2 is recovered from Equation 6.

Like Equation 2, Equation 6 is valid for any ratio a_e/a^*_∞ and therefore is not limited by the LEFM condition like Equation 3.

Figure 3 illustrates the asymptotic solution of Equation 6 together with the two asymptotic limits. Let us fix the size of a small SENT specimen, i.e. W = constant, and begin with $\alpha \approx 0$. Equation 6 gives $\sigma_n = f_t$. The specimen front face has the dominant influence for α-ratio < 0.2. Increasing the α-ratio to around 0.2 to 0.4, the specimen will show the least boundary influence. Further increasing the α-ratio beyond 0.4, the specimen back face begins to dominate, and the equivalent crack a_e from Equation 5 begins to decrease. As a result, the nominal strength σ_n turns back towards the tensile strength f_t. When α is close to 1, the condition that $\sigma_n = f_t$ is achieved again.

2.4 *Small SENT specimen & large plate*

The geometry factor $Y(a)$ for SENT specimens can be found in (Tada et al 2000). Therefore, the equivalent crack a_e can be calculated from Equation 5 (Duan & Hu 2003c).

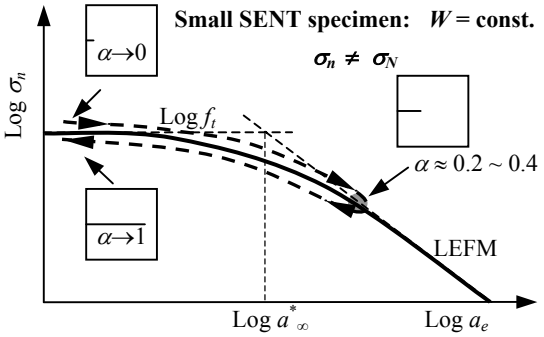

Figure 3. Asymptotic boundary effect curve for small specimens of a fixed size W and the full α-ratio range from 0 to 1. Both the front (α-ratio → 0) and back (α-ratio → 1) faces show the same boundary effect.

Figure 4(a) shows the non-dimensional plot of σ_n/f_t and a/a^*_∞. If the relative specimen size $W/a^*_\infty = 1$, the crack a ($\le W$) does not have any influence on the fracture strength, and $\sigma_n = f_t$. If the relative specimen size $W/a^*_\infty = 100$, the asymptotic quasi-brittle curve of the small SENT specimen actually follows that of the large plate for $a/a^*_\infty < 1$, and then turns up towards $\sigma_n/f_t = 1$ at $a/a^*_\infty = 100$. If the relative specimen size $W/a^*_\infty = 10{,}000$, the asymptotic quasi-brittle curve of the SENT specimen follows that of the large plate for $a/a^*_\infty < 100$, and then turns up towards $\sigma_n/f_t = 1$ at $a/a^*_\infty = 10{,}000$.

However, if we use the non-dimensional plot of σ_n/f_t and a_e/a^*_∞, all the asymptotic failure curves of the small SENT specimens fall back to the quasi-brittle fracture curve of the large plate obtained from the boundary effect model. The relative specimen size W/a^*_∞ merely determines the turning point along the asymptotic curve of the large plate as shown in Figure 4(b). Using Equation 6 and the conditions that $a_e/a^*_\infty = 0.1$ and 10 as the approximate guides, three fracture regions, f_t, quasi-brittle and K_{IC}, have been identified and shown in Figure 4(b).

2.5 *Determination of f_t and K_{IC}*

As illustrated in Figure 4, normally experimental results do show the size effect (or more accurately the boundary effect). However, the size independent material constants, f_t and K_{IC} (or the specific fracture energy G_F), can still be determined by small specimens showing strong size and boundary effects. Rearranging Equation 6, it can be found that:

$$\frac{1}{\sigma_n^2} = \frac{1}{f_t^2} + \frac{1}{f_t^2} \cdot \frac{a_e}{a_\infty^*} \tag{7}$$

Note that Equation 2 shows that the reference crack a^*_∞ is defined by f_t and K_{IC}, and is a material constant. Therefore, the size effect results given in terms of σ_n and a_e can be used to determine the two important material constants: f_t and a^*_∞. From the reference crack a^*_∞, one can determine K_{IC} and then the specific fracture energy G_F.

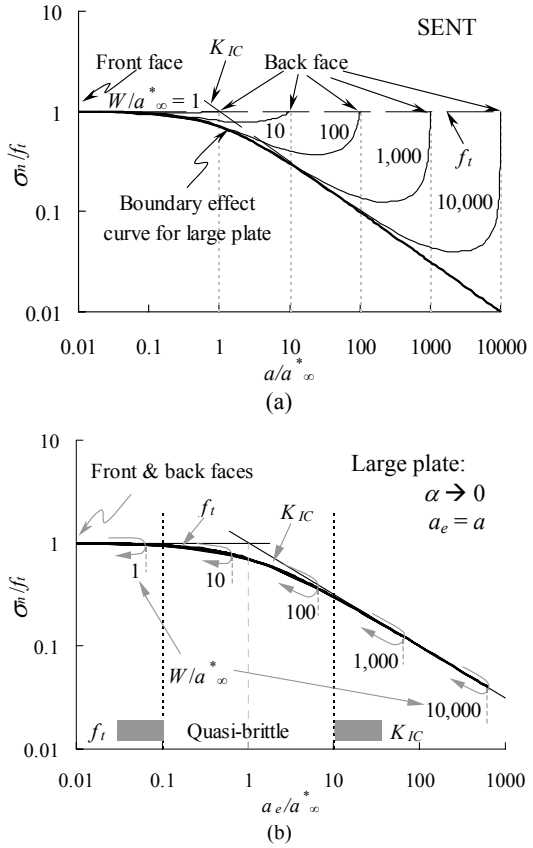

Figure 4. (a) Asymptotic boundary effect curves of large plate and small SENT specimens, with the common starting point at the front face, but different ending points at the back face depending on the specimen size W. (b) The unique asymptotic fracture curve based on that of the large plate, with the common starting point for both front and back faces. α-ratio is roughly between 0.2 and 0.4 at the turning points.

2.6 *Comparison with SEL*

The size effect law (SEL) proposed by Bažant (1984) is given by:

$$\sigma_N = \frac{A \cdot f_t}{\sqrt{1 + W/W^*}} \tag{8}$$

in which A and W^* are taken as experimental scaling parameters. While the boundary effect model, Equation 6, does not have any restriction on testing specimens, SEL or Equation 8 requires geometrically similar specimens. Rearranging Equation 6 in terms of σ_N and W, it has been found (Duan & Hu 2003a,b,c) that:

$$\sigma_N = \frac{A(\alpha) \cdot f_t}{\sqrt{1 + \dfrac{W}{\left(a^*_\infty / [B(\alpha) \cdot \alpha]\right)}}} \tag{9}$$

The two scaling parameters in SEL for the 3-p-b geometry are given by (Duan & Hu 2003a):

$$A = (1-\alpha)^2$$
$$W^* = \frac{1}{\alpha \cdot [(1-\alpha)^2]^2} \cdot \frac{1}{\pi \cdot Y^2(\alpha)} \left(\frac{K_{IC}}{f_t}\right)^2 \tag{10}$$

Clearly, both A and W^* vary with the α-ratio, the specimen geometry and the loading condition. Only under the condition of geometrically similar specimens with a fixed α-ratio, A and W^* can become constant. Therefore, the size effect observed from geometrically similar specimens and described by SEL Equation 8 is only a special case of the boundary effect model Equation 6.

3 ANALYSIS OF EXPERIMENTAL RESULTS

3.1 *Results of notched 3-p-b concrete specimens*

The high strength concrete results from Karihaloo et al (2003) are selected. The 3-p-b specimen details and results are listed in Table 1.

Specimens listed in Table 1 are not geometrically similar, except for a fixed α-ratio. However, following Equation 7, all the results in Table 1 can be presented in a single graph in terms of σ_n of and a_e, and shown in Figure 5. The geometry factor $Y(\alpha)$ in Equation 5 can be found in (ASTM 1990). The well-defined straight line in Figure 5 from the experimental results shows that f_t = 10.96 MPa, a^*_∞ = 5.72 mm and K_{IC} = 1.65 MPa√m. The elastic modulus E = 40.45 GPa has been given in (Karihaloo et al 2003) so that the size independent specific fracture energy G_F = 66.9 N/m. It should be mentioned that three different sets of geometrically similar specimens are used in Figure 5. Therefore, Figure 5 proves that it is not necessary to use only

geometrically similar specimens to study the quasi-brittle fracture transition or size effect. Specimens of any geometry and size under any loading condition can all be used since all the quasi-brittle fracture strength results determine the same material constants: the tensile strength f_t and the reference crack a^*_∞.

Table 1. Notched 3-p-b specimens

W mm	α	a_e mm	σ_N MPa	σ_n MPa
200	0.050	7.169	6.84	7.58
400	0.050	14.34	5.40	5.98
100	0.100	5.308	6.54	8.07
200	0.100	10.62	5.28	6.52
400	0.100	21.23	4.14	5.11
75	0.300	4.700	3.78	7.71
150	0.300	9.400	3.24	6.61
300	0.300	18.80	2.52	5.14

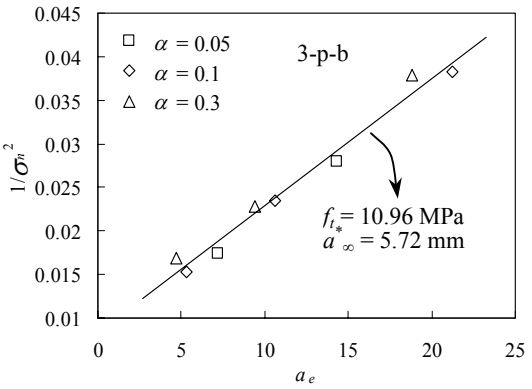

Figure 5. The linear relation of Equation (7) used to determine the two material constants f_t and a^*_∞.

Figure 6(a) shows the asymptotic solution of Equation 6 together with the experimental results and two asymptotic limits: f_t and K_{IC} criteria. Figure 6(b) shows the corresponding SEL curves from Equation 9. Clearly, the SEL equations are α-ratio dependent, and the asymptotic curves for very small α-ratios (e.g. 0.01) can be very different. That is the reason why the application of SEL requires geometrically similar specimens as in this case only a fixed α-ratio is dealt with.

3.2 *Results of un-notched 3-p-b specimens*

The un-notched 3-b-p results of the high strength concrete were also reported by Karihaloo et al (2003). The nominal strength σ_N and the corresponding specimen size W are listed in Table 2. Figure 7 shows the notched and un-notched results together with the predictions from the boundary effect model Equation 9. Interestingly, the theoretical prediction with α-ratio = 0.012 gives a good approximation to the un-notched results.

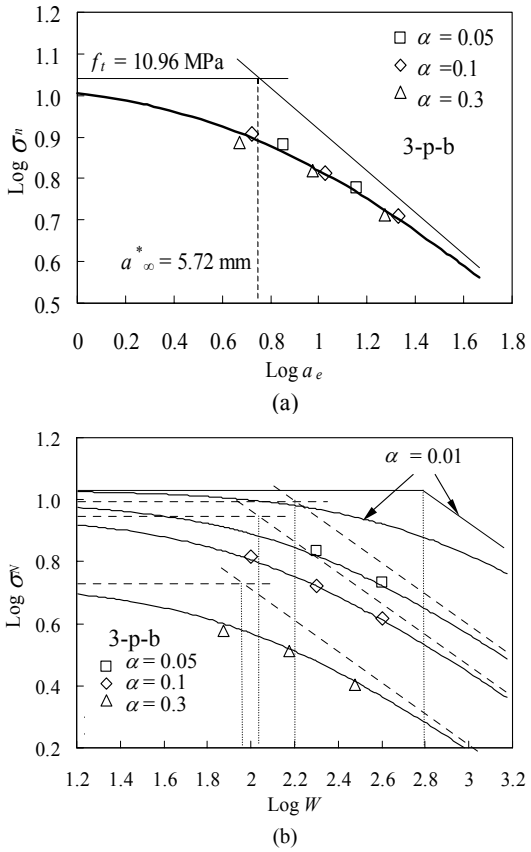

Figure 6. (a) Asymptotic fracture curve based on Log σ_n – Log a_e, and (b) curves based on Log σ_N – Log W.

Table 2. Un-notched 3-p-b specimens

W mm	σ_N MPa	α	a_e mm	σ_n MPa
50	11.28	0.012	0.5540	11.56
75	9.54	0.012	0.8309	9.77
100	9.84	0.012	1.1079	10.08
150	9.78	0.012	1.6619	10.02
200	9.12	0.012	2.2158	9.34
300	8.28	0.012	3.3237	8.48
400	8.46	0.012	4.4317	8.67

The recent work (Duan & Hu 2003a) has discussed and established the correlation between the pre-existing small defects in un-notched specimens and shallow notches in notched specimens of a small α-ratio. The key argument is that un-notched specimens do contain micro-defects. Statistically, larger specimens contain bigger defects and thus have lower strength results. If the pre-existing defects are treated as small edge cracks, equivalent

shallow notches can be defined. Geometrically similar specimens with a very small α-ratio can thus be assumed for un-notched specimens. This argument has been illustrated in Figure 8 (Duan & Hu 2003a).

The correlation between the Weibull strength distribution and defect size distribution can be found in previous publications (Hu et at 1985, 1988, Hu 1988, 1989). Assuming the equivalent α-ratio = 0.012 can be used for the un-notched specimens, the equivalent a_e and σ_n can be worked out, and they are also listed in Table 2.

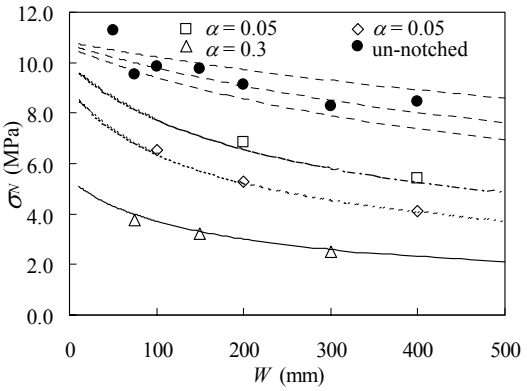

Figure 7. Quasi-brittle fracture curves based on $\sigma_n - W$, showing the tensile strength f_t for $W \to 0$, un-notched results having very small α-ratios

Figure 6(a) can then be re-plotted by including the un-notched specimens with natural flaws, and is shown in Figure 9. Clearly, the asymptotic limit of f_t = 10.96 MPa determined from the notched specimens has been confirmed by those un-notched results. This finding is significant because it shows that the tensile strength can indeed be determined from notched specimens showing strong size effect.

Interestingly, the notched and un-notched results shown in Figure 9 are spread perfectly over almost the entire fracture region from the strength region through the quasi-brittle fracture region to finally the LEFM region. Close to the region $a_e \approx a^*_\infty$ in Figure 9, there are results from the un-notched specimens with W = 400 mm and the notched specimens with W = 100 mm and α-ratio = 0.1, and the notched specimens with W = 75 mm and α-ratio = 0.3. Therefore, specimens of different sizes can indeed have a similar equivalent crack a_e, which once again shows that the specimen size W alone is not enough to specify the quasi-brittle fracture transition. The boundary and size effects need to be considered together.

Un-notched specimens with distributed micro-defects

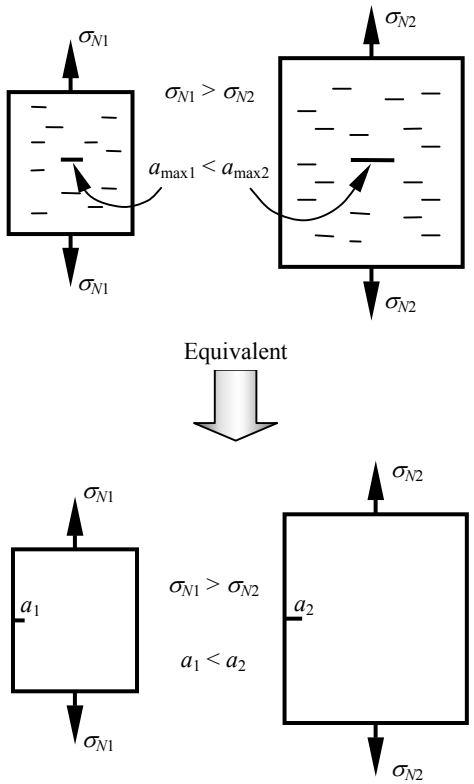

Geometrically similar specimens (α = constant)
with equivalent small α-ratio ≈ 0.01

Figure 8. The equivalence of un-notched specimens and geometrically similar specimens with shallow notches.

4 SEPARATION OF QUASI-BRITTLE FRACTURE REGION FROM f_t AND K_{IC}

Equation 6 shows that the strength criterion applies if $a_e/a^*_\infty << 1$, and the fracture toughness criterion applies if $a_e/a^*_\infty >> 1$. Therefore, for convenience, $a_e/a^*_\infty = 0.1$ can be taken as the separation between the strength and quasi-brittle fracture regions, and $a_e/a^*_\infty = 10$ can be taken as the separation between the quasi-brittle and brittle fracture regions.

The a_e/a^*_∞ ratio as a function of the α-ratio and relative size ratio W/a^*_∞ is shown in Figure 10 (Duan & Hu 2003a) for the standard 3-p-b geometry shown in Figure 1. The quasi-brittle fracture region has been clearly separated from the tensile strength f_t and fracture toughness K_{IC} regions. In general, the a_e/a^*_∞ ratio increases with increasing size ratio W/a^*_∞, confirming the common size effect. However, as shown in Figure 10, the size ratio

W/a^*_∞ itself is not enough to determine the quasi-brittle fracture transition.

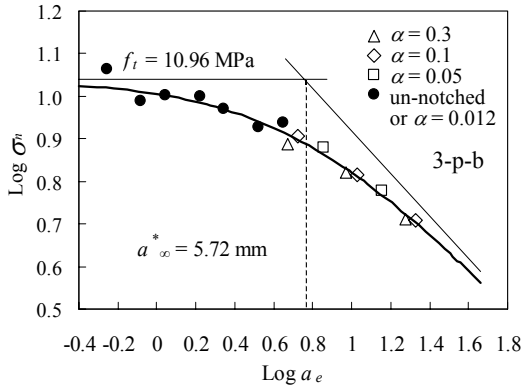

Figure 9. Asymptotic fracture curve including notched and un-notched results.

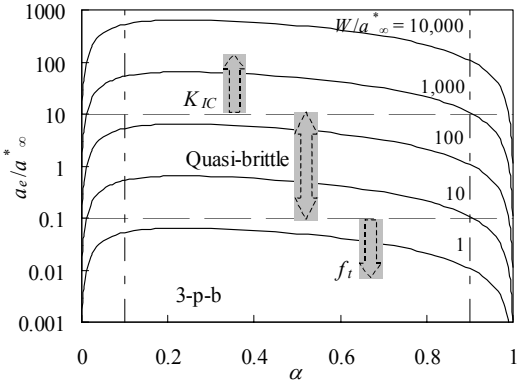

Figure 10. Material independent quasi-brittle fracture curves of 3-p-b specimens

For instance, for large specimens with the size ratio of W/a^*_∞ = 1,000, the K_{IC} criterion clearly applies within the α-ratio range of 0.01 to 0.9. However, the same specimens can indeed experience quasi-brittle fracture if they only contain very shallow and deep notches with α-ratios less than 0.01 or bigger than 0.9. Furthermore, they can even experience the pure strength criterion controlled fracture if the α-ratio $\rightarrow$ 0 or $\rightarrow$ 1. The boundary influence from the front and back faces is clearly evident from Figure 10. Interestingly, even the size effect shown in Figure 10 is obtained through the boundary effect model or Equation 6.

It is clear from Figures 4 and 10 that the boundary effect model, Equation 6, can be used to describe the three distinct fracture regions. The usefulness of the reference crack a^*_∞ defined by the asymptotic analysis of the large plate is clearly demonstrated.

5 DISCUSSION AND CONCLUSIONS

The first important step of the present boundary effect model is to clearly define two distinct nominal strengths: σ_N, which ignores the presence of a crack, and σ_n, which considers the presence of a crack. σ_n is used in the boundary effect model Equation 6, and σ_N is adopted in SEL Equation 8.

The second important step of the boundary effect model is to use two well-defined material constants, f_t and a^*_∞, *as* the scale constants. SEL uses two empirical parameter A and W^*, which are known to vary with specimen geometry and loading conditions as shown by Equation 10.

The third important step of the boundary effect model is to introduce the equivalent crack a_e, which, together with σ_n, transforms the boundary effect of small specimens to that of a large plate.

The final result is that a unique asymptotic curve is established by the boundary effect model, which is independent of the specimen size, geometry and loading condition. In contrast with the boundary effect model, the asymptotic solution of SEL varies with the specimen geometry and loading condition.

An important progress made by the present boundary effect model is that clear and explicit expressions of A(α) and $W^*(\alpha)$ are provided. As a result, A and W^* used in SEL are no longer empirical parameters, and SEL actually becomes a special case of the boundary effect model dealing exclusively with geometrically similar specimens with a fixed α-ratio. Unlike SEL that has been acclaimed to be valid only approximately in the range of $0.22 \le W/W^* \le 4.5$ (Bažant & Li 1996), the current boundary effect model is not limited by such a condition, and is valid for $0 \le W/W^* \le \infty$.

Using the boundary effect model Equation 6, one can work out important material constants f_t and a^*_∞ (and then K_{IC}, and the size independent specific fracture energy G_F) from size dependent experimental results. Previously, SEL Equation 8 would only yield two empirical parameters A and W^* varying with the loading conditions and specimen geometry and α-ratio. This conclusion on the current boundary effect model is significant as the maximum load test is probably the simplest test method in comparison with the direct tensile test and RILEM (1985) recommended test for the specific fracture energy G_F.

Previously, SEL Equation 8 cannot deal with the size-effect on the nominal strength of un-notched specimens. The present boundary effect model can

adequately describe the size-effect on the nominal strength of the un-notched specimens by correlating the distributed defects to the equivalent shallow notches. The Weibull strength and statistical flaw analysis (Hu et at 1985, 1988, Hu 1988, 1989), provides a sound physical basis for the correlation.

Finally, the theoretical quasi-brittle curves shown in Figure 4(b) provide the most direct proof that the common size effect is actually the boundary effect defined by the asymptotic boundary effect solution of the large plate for which the specimen front face, rather than the size, influences the quasi-brittle fracture transition. The distance of the crack-tip FPZ (proportional to the reference crack a^*_∞) to either the specimen front or back boundary is measured by the crack length a itself or the uncracked ligament (W-a). When geometrically similar specimens (with a constant α-ratio) are selected, the increase in size W naturally leads to the increase in FPZ's distance to the boundaries. As a result, the so-called "size effect" is observed, which in reality shows the specimen boundary influence from either the front or back faces.

The same boundary effect argument has also been used to explain the size effect on the specific fracture energy G_F specified by RILEM (1985) in a separate contribution to the conference (Duan et al, 2004) based on our previous work (Hu 1990, Hu & Wittmann 1992, Duan et al 2002, 2003b). The boundary effect model on G_F has also been proven by other material systems, such as an adhesive layer sandwiched between two non-yielding substrates (Duan et al 2003a).

6 ACKNOWLEDGEMENTS

The financial support from the Australian Research Council (ARC) under the scheme of Discovery Grant is acknowledged.

REFERENCES

ASTM E399-90, Standard test method for plane-strain fracture toughness testing of high strength metallic materials. Philadelphia: Amer Soc Testing Mater; 1990.

Bažant, Z.P. 1984. Size effect in blunt fracture: concrete, rock, metal. *Journal of Engineering Mechanics (ASCE)* 110(4): 518-535.

Bažant, Z.P & Li, Z. 1996. Zero-brittleness size-effect method for one-size fracture test of concrete. *Journal of Engineering Mechanics (ASCE)* 122: 458-468.

Carpinteri, A. 1994. Fractal nature of material microstructure and size effects on apparent mechanical properties. *Mechanics of Materials* 18: 89-101.

Duan, K. & Hu, X.Z. 2002. Asymptotic analysis of boundary effects on fracture properties of notched bending specimens of concrete. In A.V. Dyskin, X.Z. Hu, & E. Sahouryeh (eds.), *Structural Integrity and Fracture (Proc. Int. Conf. on Struct. Integrity Fract. SIF 2002)*: 19-24. Lisse, Netherlands: A.A.Balkema Publishers.

Duan, K. & Hu, X.Z. 2003a. Scaling of quasi-brittle fracture: boundary effect. Submitted to *Engineering Fracture Mechanics* (18 July 2003).

Duan, K. & Hu, X.Z. 2003b. Boundary effect on quasi-brittle fracture of compact tension specimens. Submitted to *Engineering Fracture Mechanics* (8 August 2003).

Duan, K. & Hu, X.Z. 2003c. Quasi-Brittle Fracture of Single Edge Notched Tensile Specimen and Large Plate. To be published.

Duan, K., Hu, X.Z. & Mai, Y.W., 2003a. Substrate constraint and adhesive thickness effects on fracture toughness of adhesive joints. *Journal of Adhesive Science and Technology*, (in press).

Duan, K., Hu, X.Z. & Wittmann, F.H. 2002. Explanation of size effect in concrete fracture using non-uniform energy distribution. *Materials and Structures* 35: 326-331.

Duan, K., Hu, X.Z. & Wittmann, F.H., 2003b. Boundary Effect on Concrete Fracture and Non-Constant Fracture Energy Distribution. *Engineering Fracture Mechanics* 70: 2257-2268.

Duan, K., Hu, X.Z. & Wittmann, F.H. 2004. Boundary effects and fracture of concrete. In this *Proceeding*.

Hu, X.Z. 1988. Statistical Fracture of Brittle Materials. Ph.D thesis, Sydney University, Sydney, Australia.

Hu, X.Z. 1989. Flaw analysis in time-dependent fracture for cementitious materials. In S.P. Shah, S.E. Swarts & B. Barr (eds.), *Fracture of Concrete and Rock*: 307-316. England: Elsevier.

Hu, X.Z., 1998. Size effects in toughness induced by crack close to free edge. In H. Mihashi, & K. Rokugo (eds.), *Fracture Mechanics of Concrete Structures (Proc. Framcos-3)*: .2011-2020. Freiburg: Aedificatio Publishers.

Hu, X.Z., 2002. An asymptotic approach to size effect on fracture toughness and fracture energy of composites. *Engineering Fracture Mechanics* 69: 555-564.

Hu, X.Z., Cotterell, B. & Mai, Y.W. 1985. A statistical theory of fracture in a two-phase brittle material. *Proc R Soc Lond* A 401: 251-265.

Hu, X.Z., Mai, Y.W. & Cotterell, B. 1988. A statistical theory of time-dependent fracture for brittle materials. *Philos Mag* 58: 299-324.

Karihaloo B.L., Abdalla H.M. & Xiao Q.Z. 2003. Size effect in concrete beams. *Engineering Fracture Mechanics* 70: 979-993.

RILEM TC-50 FMC 1985. Determination of the fracture energy of mortar and concrete by means of three-point bend tests on notched beams. *Materials and Structures* 18: 287-90.

Tada H., Paris P.C. & Irwin G.R. 2000. The Stress Analysis of Cracks Handbook (3rd Ed.). New York: ASME Press.